

BIOMECHANICS OF CHIASMAL COMPRESSION: SENSITIVITY OF THE MECHANICAL BEHAVIOURS OF NERVE FIBRES TO VARIATIONS IN MATERIAL PROPERTY AND GEOMETRY

XIAOFEI WANG^{*}, ANDREW J. NEELY[†], GAWN G. MCILWAINE[§] AND
CHRISTIAN J. LUECK[‡]

^{*} School of Engineering and Information Technology, University of New South Wales Canberra, ACT 2602, Australia, xiaofei.wang@student.adfa.edu.au, seit.unsw.adfa.edu.au

[†] School of Engineering and Information Technology, University of New South Wales Canberra, ACT 2602, Australia, a.neely@adfa.edu.au, seit.unsw.adfa.edu.au

[§] Queen's University Belfast and Belfast Health and Social Care Trust, Belfast, Northern Ireland, UK, gawn.mcilwaine@belfasttrust.hscni.net, www.belfasttrust.hscni.net

[‡] The Canberra Hospital and Australian National University, Canberra, ACT, Australia, christian.lueck@act.gov.au, health.act.gov.au

Key Words: *Bitemporal Hemianopia, Chiasmal Compression, Finite Element Modelling, Multi-scale, Design of Experiment.*

Abstract. The mechanism of bitemporal hemianopia is still unclear. Previous research suggested that the nerve fibre packing pattern may contribute to the selective damage of nasal (crossed) nerve fibres. Numerical models were built using finite element modelling to study the biomechanics of optic nerve fibres. The sensitivity of the mechanical behaviours of the nerve fibres to variations of five parameters in the nerve fibre model were investigated using design of experiments (DOE). Results show that the crossing angle is a very significant factor that affects a wide range of responses of the model. The strain difference between the crossed and the uncrossed nerve fibres may account for the phenomenon of bitemporal hemianopia. This work also highlights the need for more accurate material properties of the tissues in the model and an improved understanding of the microstructure of the optic chiasm.

1 INTRODUCTION

In the human visual system, information from the right visual field (VF) is processed by the left side of the brain and *vice versa*. To achieve this, there is a partial crossing of optic nerve fibres in the optic chiasm. The nasal (crossed) fibres lie centrally in the chiasm and cross to the opposite side of the brain while the temporal (uncrossed) fibres pass directly back

to the same side of the brain in the lateral parts of the chiasm. Compression of the chiasm typically produces a pattern of visual loss known as a bitemporal hemianopia due to selective damage to the crossed nerve fibres which arise from the nasal hemiretinae (and hence represent the temporal visual fields).

In bitemporal hemianopia vision is lost in the temporal half of the VFs of both the right and left eyes. This pattern of visual loss is highly localizing to the chiasm and it has many known causes, most of which involve compression of the chiasm. Rarer causes of chiasmal compression include craniopharyngiomas, germinomas, metastatic tumours, and giant carotid aneurysms ^[1,2] but the most common cause is a pituitary tumour which compresses the chiasm from below as it grows up out of the pituitary fossa (a depression of bone housing the pituitary gland) ^[1,3]. Vision may recover rapidly after surgical decompression ^[4,5] but this is not always the case. Although the fact that chiasmal compression by a pituitary tumour results in bitemporal hemianopia is well-recognized, the reason why compressive lesions of the chiasm selectively damage the crossed nasal nerve fibres is still not clear. Previous theories suggesting that damage is due to the effects of stretching ^[6] or alteration in blood supply ^[7] cannot explain the sharp cutoff along the vertical meridian of the visual fields which is observed clinically.

In a previous study, we used finite element modelling (FEM) to simulate optic chiasm compression at different length scales (Figure 1). The results of the macroscopic model agreed well with the limited experimental results available. Unfortunately, the data necessary to populate the various parameters used in the microscopic nerve fibre model are scarce in the literature and, even when these parameters are reported, the values can vary considerably from study to study. Accordingly, this paper investigated the sensitivity of models describing the mechanical behaviour of nerve fibres to variations in the values chosen to represent relevant material properties and geometry.

2 METHODS AND MATERIALS

Design of Experiments (DOE) was used to investigate the impact of uncertainty of these factors on the output, or response, of the RVE model. DOE is an established tool which permits better understanding and control of variability in manufactured products. There has been a recent increase in interest in using DOE for sensitivity analysis in biomechanics ^[8-10]. In particular, DOE provides information about the effects of possible interactions between factors, something which is not obtainable when testing one factor at a time (OFAT).

The chiasmal compression model was based on our previous research and is briefly described here. The geometry of the chiasm was derived from a 3D-reconstruction of the head slices available at the 'US visible human project' ^[11]. The optic chiasm, optic nerves and optic tracts were considered to be composed of isotropic nerve tissue surrounded by a pial sheath. A spherical balloon representing a growing tumour was inflated first and then translated inferior-superiorly so as to elevate and compress the chiasm from below (Figure 1). Inspection of the MRI scans of patients experiencing chiasmal compression ^[12-14] indicates that it is reasonable to use an initially-spherical balloon to represent the tumour. Micro-scale models were subsequently generated using representative volume elements (RVE) to investigate the strain distributions within nerve fibres. The two models are schematically illustrated in Figure 1. The strain state of a point in the central part of the chiasmal model was

extracted and applied to the RVE models to generate boundary conditions (Figure 2) [15,16].

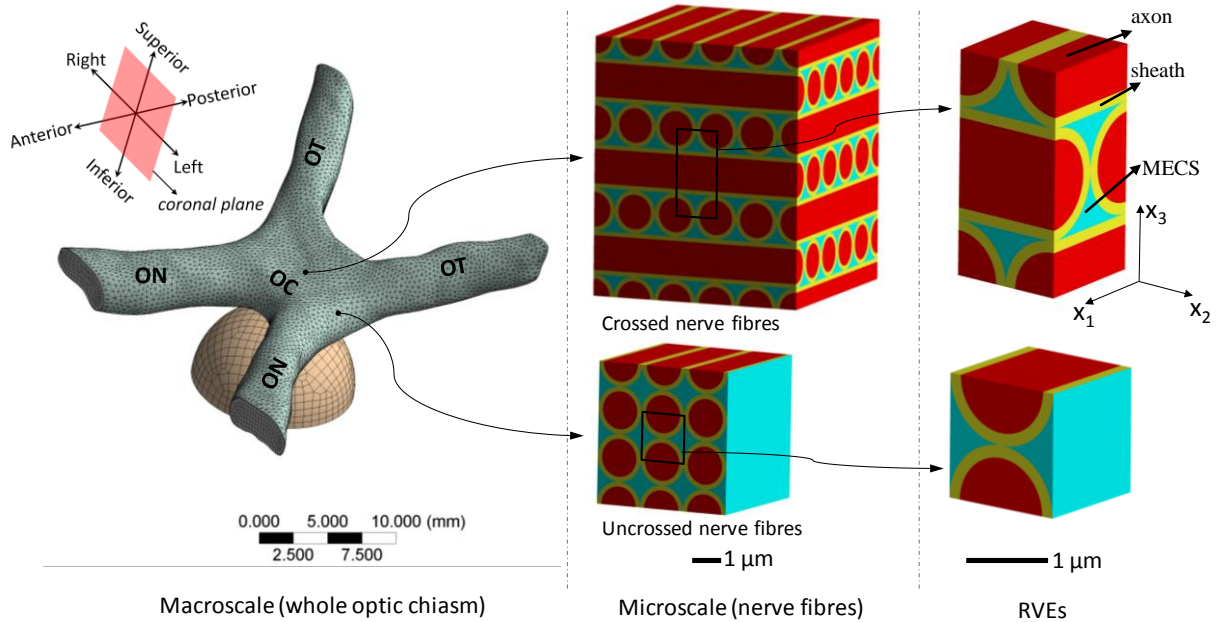


Figure 1. The macroscopic model of the optic chiasm and tumour and the microscopic RVE models. (OC: optic chiasm; ON: optic nerve; OT: optic tract; MECS: material of the extracellular space.)

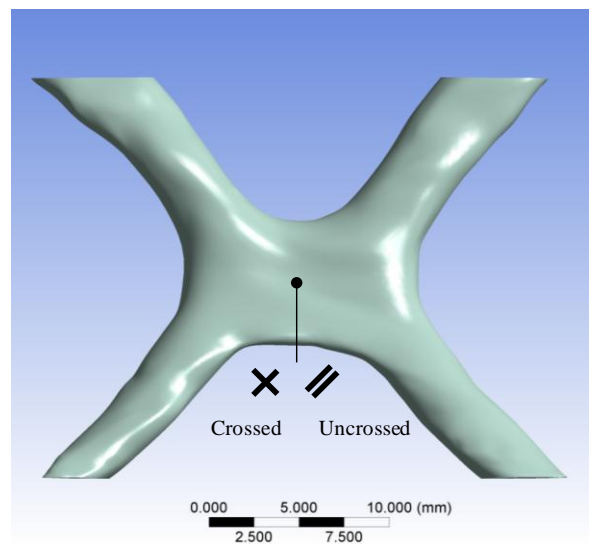


Figure 2. The strain state of a point in the chiasm was applied on the RVEs.

2.1 Representative volume elements

A RVE corresponds to a microstructural subdomain that is representative of the entire

microstructure ^[17]. The RVE can repeat itself to form the larger-scale structure. Therefore, periodic boundary conditions must be adopted to include the effect of the surrounding medium (RVEs). The strain components from the macroscopic model and the periodic boundaries were applied to the RVE model using constraint equations. The computational simulations were performed using ANSYS Mechanical APDL (Ansys, Inc., Canonsburg, PA). The structures of the RVE are indicated in Figure 1.

2.2 Periodic boundary conditions

Xia *et al.* ^[18] developed a periodic boundary condition for RVEs which can easily be used in FEM analysis. The displacements of the boundary surfaces of a RVE are given by:

$$u_i = \bar{\epsilon}_{ik}x_k + u_i^* \quad (1)$$

where x_k is the Cartesian coordinate of a point, $\bar{\epsilon}_{ik}$ is the average strain and u_i^* is the periodic part of the displacement on the boundary faces which is unknown. Considering two opposite faces with their normal along the x_j axis (Figure 1), the displacements on these two faces can be written as:

$$u_i^{j+} = \bar{\epsilon}_{ik}x_k^{j+} + u_i^{*j+} \quad (2)$$

$$u_i^{j-} = \bar{\epsilon}_{ik}x_k^{j-} + u_i^{*j-} \quad (3)$$

where j^+ refers to the positive x_j direction and j^- refers to the negative x_j direction.

As opposite faces in the deformed RVE should have the same shape so that they can repeat to form a continuous body, the local fluctuations u_i^{*j+} and u_i^{*j-} must be identical on these two faces. Therefore, the relative displacement between these two faces is:

$$u_i^{j+} - u_i^{j-} = \bar{\epsilon}_{ik}(x_k^{j+} - x_k^{j-}) = \bar{\epsilon}_{ik}\Delta x_k^j \quad (4)$$

where $\bar{\epsilon}_{ik}$ is the average strain which is obtained from the macroscopic model and Δx_k^j are known from the geometry of the RVE.

Equation (4) can be applied to the RVE using constraint equations in ANSYS. In order to apply these constraint equations, the mesh on opposite faces of the RVE had to be identical. This was achieved by meshing one face first and then copying the mesh to the corresponding opposite face. Because there were so many nodes involved, the ANSYS Parametric Design Language was used to find each corresponding node pair and impose constraint equations on them. The node at one corner of the model was fixed to avoid rigid body motion. As large deflection analysis was used to help convergence, dummy nodes in ANSYS were used to allow the deformation applied to the RVE to increase gradually.

Using the procedures described above, strain loads from the macro-scale model were imposed on the RVE, which allowed transition of the actual strains from the macroscopic deformation field to the micro level.

3 DESIGN OF EXPERIMENTS

A five-factor two-value, or two-level, full factorial analysis was designed to investigate the effect of five parameters in the RVE model systematically. Full factorial analysis was used to

allow examination of the effects of individual factors and all possible interactions of those factors. The five factors and their levels are listed in Table 1. The definition of these factors will be introduced later. The high and low levels of a given factor were based on a reasonable range derived from data reported in the literature.

Table 1. Factors and their levels of the DOE study

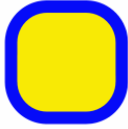
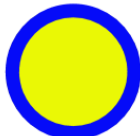
Factor	Factor name	Low level (-1)	High level (1)
A	Cross-sectional shape	 Rounded-cornered square	 circle
B	g-ratio	0.6	0.8
C	Sheath stiffness	1/3 (of the axon')	1/2 (of the axon')
D	MECS stiffness	1/20 (of the axon')	1/10 (of the axon')
E	Crossing angle	0 ° (parallel)	90 ° (perpendicular)

Table 2 shows the design matrix that reflects all possible combinations of high and low levels for each factor. The high and low levels of each factor were coded as +1 and -1, respectively. A total of 32 (2^5) simulations were performed based on the configurations in Table 2 using ANSYS, and the simulation responses were then processed using Minitab which is a statistics package (Version 15, State College, PA).

Two cross-sectional shapes were chosen as either a circle or a rounded-corner square. These geometries were based on the microscopic appearance of nerve fibres within the optic nerve. Both shapes had the same cross-sectional area which was based on the nerve fibre area quoted in the literature^[19]. Note that the change of cross-sectional shape necessarily resulted in a change in the volume fraction of nerve fibres (i.e. volume of fibres / total volume of the RVE). Fibre fractions for the circular and rounded-corner square cross-sections were 78.5% and 90%, respectively. Of note, 90% is believed to be the fibre fraction in the optic nerve^[20].

The ratio of the axonal diameter divided by the diameter of the whole nerve fibre (axon plus its myelin sheath) is called the g-ratio. For mammals, the g-ratio usually varies between 0.6 and 0.8^[21,22]. In this paper, the g-ratio for nerve fibre with a rounded-corner square cross-section was calculated as the horizontal width (see figure in Table 1) of the axon divided by the width of the nerve fibre.

Both the von Mises strain and the strain value along the axonal direction (axonal strain) were reported as the latter is arguably a better measure of axonal injury in brain white matter^[15,23], although whether this applies to the chiasm is still unclear. The responses and their abbreviation are listed in Table 3.

Table 2. Design of the simulations

Simulation No.	A	B	C	D	E	Simulation No.	A	B	C	D	E
1	-1	-1	-1	-1	-1	17	-1	-1	-1	-1	1
2	1	-1	-1	-1	-1	18	1	-1	-1	-1	1
3	-1	1	-1	-1	-1	19	-1	1	-1	-1	1
4	1	1	-1	-1	-1	20	1	1	-1	-1	1
5	-1	-1	1	-1	-1	21	-1	-1	1	-1	1
6	1	-1	1	-1	-1	22	1	-1	1	-1	1
7	-1	1	1	-1	-1	23	-1	1	1	-1	1
8	1	1	1	-1	-1	24	1	1	1	-1	1
9	-1	-1	-1	1	-1	25	-1	-1	-1	1	1
10	1	-1	-1	1	-1	26	1	-1	-1	1	1
11	-1	1	-1	1	-1	27	-1	1	-1	1	1
12	1	1	-1	1	-1	28	1	1	-1	1	1
13	-1	-1	1	1	-1	29	-1	-1	1	1	1
14	1	-1	1	1	-1	30	1	-1	1	1	1
15	-1	1	1	1	-1	31	-1	1	1	1	1
16	1	1	1	1	-1	32	1	1	1	1	1

According to the literature, the stiffness of the myelin sheath is two to three times softer than the axon [20,24,25]. The material properties of MECS (material of the extracellular space) were assumed to be approximately as soft as cerebrospinal fluid. All material properties were modified from those of the axon. The material properties of the axon were represented using a second-order Ogden hyperelastic model ($\mu_1 = 1044$ Pa, $\mu_2 = 1183$ Pa, $\alpha_1 = 4.309$ and $\alpha_2 = 7.736$), based on the material properties of brain white matter [26].

Table 3. Simulation responses and their abbreviations

Response description	Abbreviation
Maximum von Strain of the axon	M_VON_A
Maximum axonal strain of the axon	M_AXONAL_A
Maximum von Strain of the sheath	M_VON_S
Maximum axonal strain of the sheath	M_AXONAL_S

4 RESULTS

The responses of the 32 simulations are listed in Table 4. The effects for individual and coupled variables were analysed using Pareto charts in Minitab. The effect of an individual variable is called a main effect and the effect of coupled variables is the interaction effect. In the Pareto chart, the horizontal bars represent the effects of individual factors or interactive effects of the factors. Bar lengths exceeding the vertical line are statistically significant. The

vertical line was generated by Minitab using the method of Lenth^[27]. Because one numerical simulation yields only one set of results, there are no replications which are necessary to evaluate error in physical experiments. Lenth's method is specially designed for the study of numerical simulations to overcome this issue.

Table 4. Responses of the 32 simulations

Simulation No.	Max. von Mises strain of the axon	Max. axonal strain of the axon	Max. von Mises strain of the sheath	Max. axonal strain of the sheath
1	0.095619	0.053948	0.171405	0.056956
2	0.086273	0.053082	0.156530	0.058435
3	0.100840	0.052520	0.142738	0.057992
4	0.095726	0.051843	0.143253	0.060221
5	0.094395	0.053729	0.172719	0.053934
6	0.085791	0.053161	0.159572	0.054577
7	0.099833	0.052309	0.143009	0.054803
8	0.095244	0.051891	0.135045	0.056349
9	0.100754	0.052589	0.181271	0.057334
10	0.098719	0.054016	0.168807	0.055366
11	0.106652	0.051703	0.150942	0.055994
12	0.105354	0.052081	0.149031	0.057720
13	0.099696	0.052190	0.182781	0.054884
14	0.098397	0.053500	0.172297	0.054181
15	0.105328	0.051330	0.145314	0.054069
16	0.104942	0.051614	0.139543	0.054218
17	0.105401	0.065002	0.185658	0.076603
18	0.092370	0.066007	0.166138	0.086871
19	0.109700	0.062627	0.154227	0.085210
20	0.099665	0.067027	0.152431	0.088942
21	0.105934	0.063867	0.188000	0.069948
22	0.091748	0.064138	0.170929	0.078286
23	0.110354	0.061364	0.156133	0.069563
24	0.100175	0.064566	0.146779	0.073685
25	0.106110	0.063584	0.192016	0.092820
26	0.105250	0.070967	0.182798	0.094405
27	0.110683	0.063399	0.174352	0.095367
28	0.107683	0.069243	0.159906	0.092723
29	0.107646	0.061701	0.200742	0.075726
30	0.104451	0.068678	0.188148	0.085365
31	0.109871	0.061282	0.159097	0.079697
32	0.107528	0.065909	0.150352	0.078357

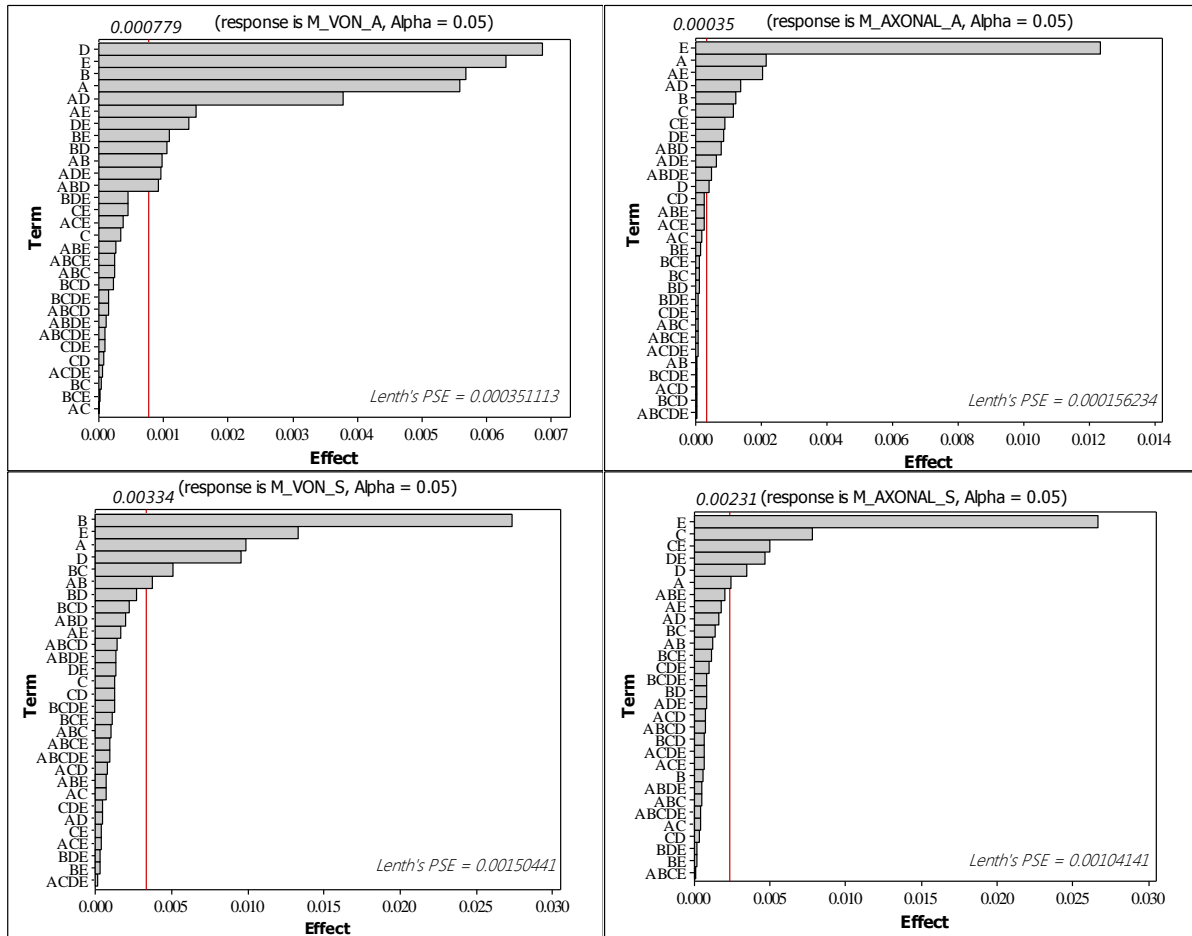


Figure 3. Pareto analysis for various responses of the model. A: cross-sectional shape; B: g-ratio; C: sheath stiffness; D: MECS stiffness; E: crossing angle. Only the 30 largest effects are shown.

Among the four responses listed in Table 3, two (M_AXONAL_A, M_AXONAL_S) were predominantly affected by the crossing angle. For these responses, the effect of crossing angle was 472% and 240% greater than that of the second most important factor, respectively.

For the remaining two responses (M_VON_A, M_VON_S), crossing angle was ranked as the second most significant factor, 8.2% and 51.2% less significant than the most significant factors, respectively. For M_VON_S, g-ratio was the most significant factor while MECS stiffness was the most significant response for M_VON_A.

5 CONCLUSIONS

The effect of varying five parameters of the nerve fibre model was systematically analysed using DOE. The results indicated that crossing angle was the leading factor influencing all the responses of the model. It should be noted that the range of variation of the g-ratio and the stiffness of materials in this sensitivity study were based on the ranges reported in the literature derived from different animals. However, for an individual person, the g-ratio will

vary only slightly, or even remain constant^[22]. In other words, a large variation of g-ratio from 0.6 to 0.8 would be unlikely to occur in a single optic chiasm. Similarly, the MECS stiffness would be likely to remain fairly constant in a single individual.

We can conclude that, for any given g-ratio and MECS stiffness, the crossing angle is the most significant factor that affects a wide range of responses of the model. It can be seen from Figure 3 that an increase in crossing angle from 0° to 90° resulted in greater values of all four responses. Thus, the strain difference between crossed and uncrossed nerve fibres may well account for the phenomenon of bitemporal hemianopia.

Interestingly, compared to the crossing angle and g-ratio, cross-sectional shape was not a very significant factor though it should be noted that only two cross-sections were considered in this study. In reality, though, the actual cross-sectional geometry of nerve fibres is significantly more complicated than the two regular shapes used in this study.

It should be pointed out that, in this study, fibre orientation and the location of macroscopic strain were fixed, as in Figure 2. The effect of altering orientation in the RVE models was not considered. Before this can be done, a greater understanding of the microstructure of the optic chiasm is needed in order to determine the actual orientation of the nerve fibres within the chiasm. In addition, this work highlights the need for more accurate information about the material properties of the tissues used in the model.

REFERENCES

- [1] Blumenfeld H. *Neuroanatomy through Clinical Cases*. Sunderland, Massachusetts: Sinauer Associates, 2010.
- [2] Oliver L. Compression of Optic Chiasm by an Intracranial Carotid Aneurysm. *Proceedings of the Royal Society of Medicine-London* 1964;**57**(7):590-90.
- [3] Kosmorsky GS, Dupps Jr WJ, Drake RL. Nonuniform Pressure Generation in the Optic Chiasm May Explain Bitemporal Hemianopsia. *Ophthalmology* 2008;**115**(3):560-65.
- [4] Kayan A, Earl CJ. Compressive lesions of the optic nerves and chiasm. Pattern of recovery of vision following surgical treatment. *Brain* 1975;**98**(1):13-28.
- [5] Anik I, Anik Y, Koc K, et al. Evaluation of early visual recovery in pituitary macroadenomas after endoscopic endonasal transphenoidal surgery: Quantitative assessment with diffusion tensor imaging (DTI). *Acta Neurochirurgica* 2011;**153**(4):831-42.
- [6] Hedges TR. Preservation of the upper nasal field in the chiasmal syndrome: an anatomic explanation. *Transactions of the American Ophthalmological Society* 1969;**67**:131-41.
- [7] Bergland R, Ray BS. The arterial supply of the human optic chiasm. *J. Neurosurg.* 1969;**31**(September):327-34.
- [8] Yao J, Salo AD, Lee J, Lerner AL. Sensitivity of tibio-menisco-femoral joint contact behavior to variations in knee kinematics. *Journal of Biomechanics* 2008;**41**(2):390-98.
- [9] Shen H, Li H, Brinson LC. Effect of microstructural configurations on the mechanical responses of porous titanium: A numerical design of experiment analysis for orthopedic applications. *Mechanics of Materials* 2008;**40**(9):708-20.
- [10] Malandrino A, Planell JA, Lacroix D. Statistical factorial analysis on the poroelastic material properties sensitivity of the lumbar intervertebral disc under compression, flexion and axial rotation. *Journal of Biomechanics* 2009;**42**(16):2780-88.
- [11] Mikula S, Stone JM, Jones EG. BrainMaps.org - Interactive High-Resolution Digital Brain Atlases and Virtual Microscopy. *Brains, minds & media : journal of new media in neural and cognitive science and education* 2008;**3**:bmm1426.
- [12] Fahlbusch R, Gerganov VM. Non-functional pituitary tumors. In: Kaye A, Jr EL, eds. *Brain Tumors* (Third Edition). Philadelphia: W.B. Saunders, 2012:672-91.

- [13] Egger J, Bauer MH, Kuhnt D, Freisleben B, Nimsky C. Pituitary adenoma segmentation. *Proceedings of Biosignal 2010* 2011.
- [14] Honegger J, Zimmermann S, Psaras T, et al. Growth modelling of non-functioning pituitary adenomas in patients referred for surgery. *European Journal of Endocrinology* 2008;**158**(3):287-94.
- [15] Cloots RJH, van Dommelen JAW, Nyberg T, Kleiven S, Geers MGD. Micromechanics of diffuse axonal injury: influence of axonal orientation and anisotropy. *Biomechanics and Modeling in Mechanobiology* 2011;**10**(3):413-22.
- [16] Wang XF, Wang XW, Zhou GM, Zhou CW. Multi-scale analyses of 3D woven composite based on periodicity boundary conditions. *Journal of Composite Materials* 2007;**41**(14):1773-88.
- [17] Kouznetsova V, Brekelmans WAM, Baaijens FPT. An approach to micro-macro modeling of heterogeneous materials. *Computational Mechanics* 2001;**27**(1):37-48.
- [18] Xia ZH, Zhang YF, Ellyin F. A unified periodical boundary conditions for representative volume elements of composites and applications. *International Journal of Solids and Structures* 2003;**40**(8):1907-21.
- [19] Jonas JB, Müller-Bergh JA, Schlötzer-Schrehardt UM, Naumann GO. Histomorphometry of the human optic nerve. *Investigative Ophthalmology & Visual Science* 1990;**31**(4):736-44.
- [20] Arbogast KB, Margulies SS. A fiber-reinforced composite model of the viscoelastic behavior of the brainstem in shear. *Journal of Biomechanics* 1999;**32**(8):865-70.
- [21] Guy J, Ellis EA, Kelley K, Hope GM. Spectra of G Ratio, Myelin Sheath Thickness, and Axon and Fiber Diameter in the Guinea Pig Optic Nerve. *Journal of Comparative Neurology* 1989;**287**(4):446-54.
- [22] Sherman DL, Brophy PJ. Mechanisms of axon ensheathment and myelin growth. *Nature Reviews Neuroscience* 2005;**6**(9):683-90.
- [23] Wright RM, Ramesh KT. An axonal strain injury criterion for traumatic brain injury. *Biomech Model Mechanobiol* 2012;**11**(1-2):245-60.
- [24] Lu YB, Franze K, Seifert G, et al. Viscoelastic properties of individual glial cells and neurons in the CNS. *Proceedings of the National Academy of Sciences of the United States of America* 2006;**103**(47):17759-64.
- [25] Shreiber D, Hao H, Elias R. Probing the influence of myelin and glia on the tensile properties of the spinal cord. *Biomechanics and Modeling in Mechanobiology* 2009;**8**(4):311-21.
- [26] Franceschini G. *The Mechanics of Human Brain Tissue*. University of Trento, 2006.
- [27] Lenth RV. Quick and Easy Analysis of Unreplicated Factorials. *Technometrics* 1989;**31**(4):469-73.